Interactions between Atmospheric Rivers and Warm Conveyor Belts over the North Pacific during the 2025–26 AR Reconnaissance Campaign

Center for Western Weather and Water Extremes

Benjamin Moore, Jason Cordeira, Minghua Zheng, and Marty Ralph

Center for Western Weather and Water Extremes,
Scripps Institution of Oceanography, University of California, San Diego

Contact: bem006@ucsd.edu

This work was supported by the U.S. Army Corps of Engineers and the California Department of Water Resources

Introduction

Atmospheric rivers (ARs) can supply warm, moist air into deeply ascending warm conveyor belt (WCB) airstreams.

Hypothesis: AR–WCB interactions (Fig. 1) occur frequently and represent a key pathway through which ARs can influence the dynamics and predictability of the large-scale midlatitude flow.

Approach:

1. Lagrangian trajectory analysis of ARs over the North Pacific during Dec 2025 – Mar 2026
2. An AR Recon case study utilizing data-denial forecast experiments
3. Composite analysis of AR–WCB interactions

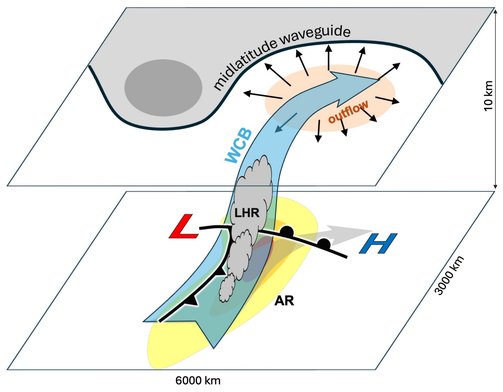

Fig. 1. Conceptual illustration of an AR–WCB interaction and its synoptic context.
Inspired by Fig. 1 of Quinting and Grams (2021).

Conclusions

- A pilot analysis for winter 2025–26 reveals that AR–WCB interactions are common over the North Pacific, with ~74% of WCB trajectories passing through an AR, underscoring ARs as a key source for moist air ascending in WCBs.
- WCB strength and diabatic heating rates tend to increase with AR intensity.
- AR–WCB interactions can promote ridge amplification along the waveguide, leading to downstream Rossby wave packet formation and growth/propagation of forecast errors.
- Ridge amplification and downstream impacts tend to be more pronounced for ARs associated with strong WCBs.
- Assimilation of AR Recon dropsondes can reduce forecast errors in the midlatitude flow associated with AR–WCB-driven ridge amplification.

Data and methods

- **Data:** ECMWF ERA5 reanalysis, MPAS data-denial experiments from AR Recon, & NOAA GEFS forecasts
- ARs tracked as 2D IVT objects at 6-h steps during Dec 2025 – Mar 2026 with the *tARget* algorithm of Guan and Waliser (2024).
- 24-h backward and 72-h forward (96-h total) trajectories released in the 1000–700-hPa layer from all grid points in ARs over the North Pacific (20–60°N, 120°E–120°W) using *LAGRANTO* (Sprenger and Wernli 2015).
- WCBs detected as 48-h trajectory segments ascending > 600 hPa.
- WCB strength quantified for each AR by the WCB trajectory count (N_{WCB}) and fraction (f_{WCB}).
- WCB components defined as:
  - *inflow*: p > 800 hPa,
  - *ascent*: 400 hPa < p < 800 hPa
  - *outflow*: p < 400 hPa

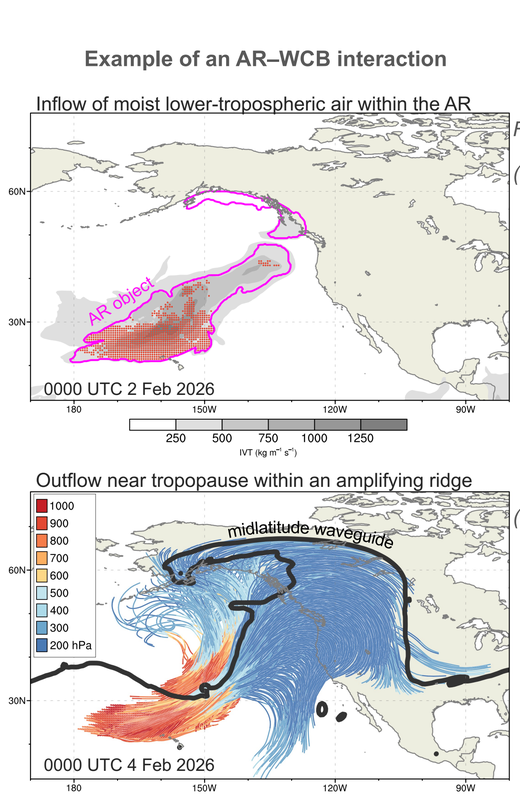

Fig 2.

(a) WCB trajectory release points (red dots) within an AR object (magenta contour) overlaid on the IVT field (gray shading)

(b) 48-h WCB trajectories (pressure shaded) released from points in (a) overlaid by the 320-K isentrope on the dynamic tropopause (2-PVU surface)

Statistical analysis for winter 2025–26

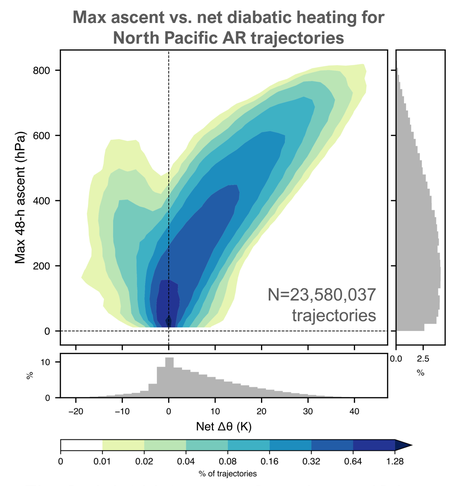

Fig. 3. Joint histogram of maximum 48-h ascent vs. net diabatic heating over that same 48-h segment for all trajectories released from North Pacific ARs.

- Trajectories from ARs frequently ascend and undergo diabatic heating, with net heating increasing with total ascent (Fig. 3).
- ~8% of AR trajectories contain a WCB.
- ~74% of all North Pac. WCB trajectories pass through an AR while in the lower troposphere (p > 700 hPa).
- WCB strength and diabatic heating rates scale with AR intensity (Fig. 4).

Fig. 4. Violin plots showing distributions for quintile bins of North Pac. AR objects stratified by mean IVT.

(a) % of AR trajectories exhibiting a WCB (i.e., WCB strength)

(b) mean net diabatic heating for all trajectories released per AR

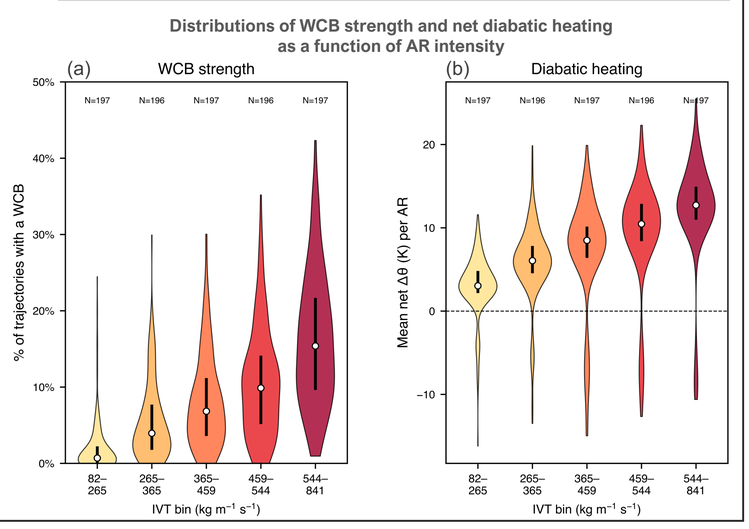

Downstream impacts and forecast uncertainty

AR Recon case study: Early February 2026

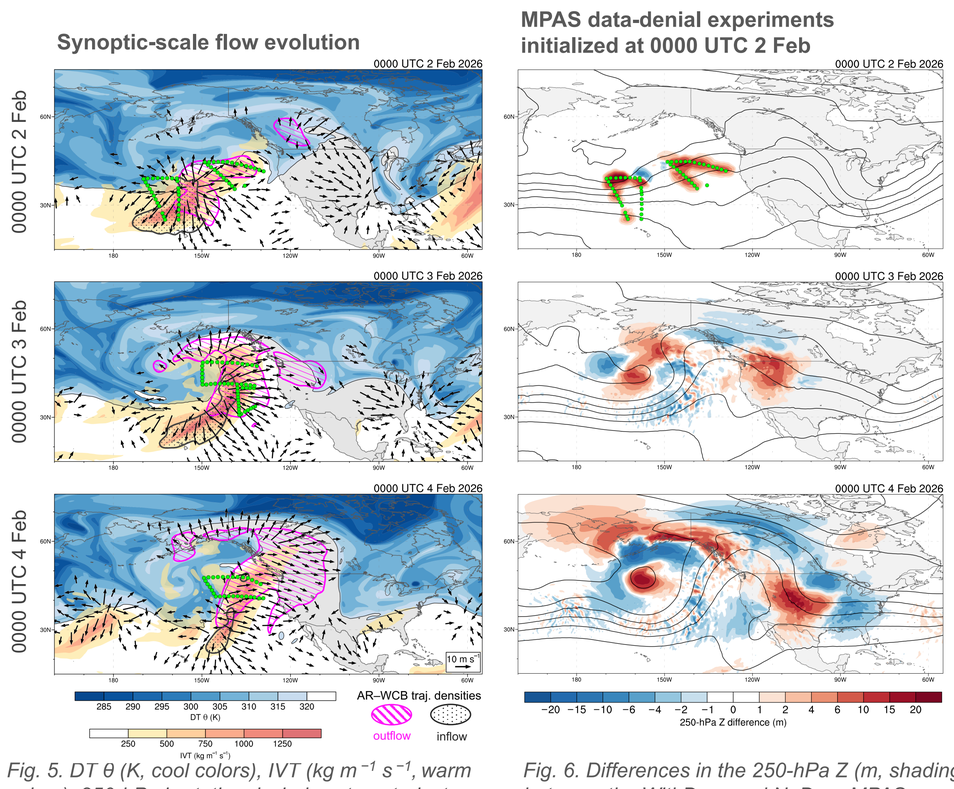

Fig. 5. DT θ (K, cool colors), IVT (kg m^{-1} s^{-1}, warm colors), 250-hPa irrotational wind vectors, trajectory densities for AR–WCB inflow (>300 trajs (10^4 km^2)$^{-1}$, black stippling) and outflow (>100 trajs (10^4 km^2)$^{-1}$, magenta hatching). Dropsonde locations in green.

Fig. 6. Differences in the 250-hPa Z (m, shading) between the WithDrop and NoDrop MPAS forecast experiments initialized at 0000 UTC 2 Feb, with the Z field from WithDrop in contours. Dropsonde locations in green.

- Ridge amplification linked to a strong AR and related WCB activity over the eastern Pacific (Fig. 5) resulted in a Rossby wave packet that extended far downstream (Fig. 7a).
- This AR and the WCB airstreams were sampled by AR Recon flights (Fig. 5).
- Comparison of MPAS forecasts initialized at 00 UTC 2 Feb with (**WithDrop**) and without (**NoDrop**) assimilated dropsondes reveals the impact of targeted observations in the AR–WCB region on the forecast Rossby wave pattern (Figs. 6 & 7).
- The WithDrop forecast exhibits error reductions in the midlatitude flow, especially over North America and the Atlantic/Europe region (Fig. 7d)

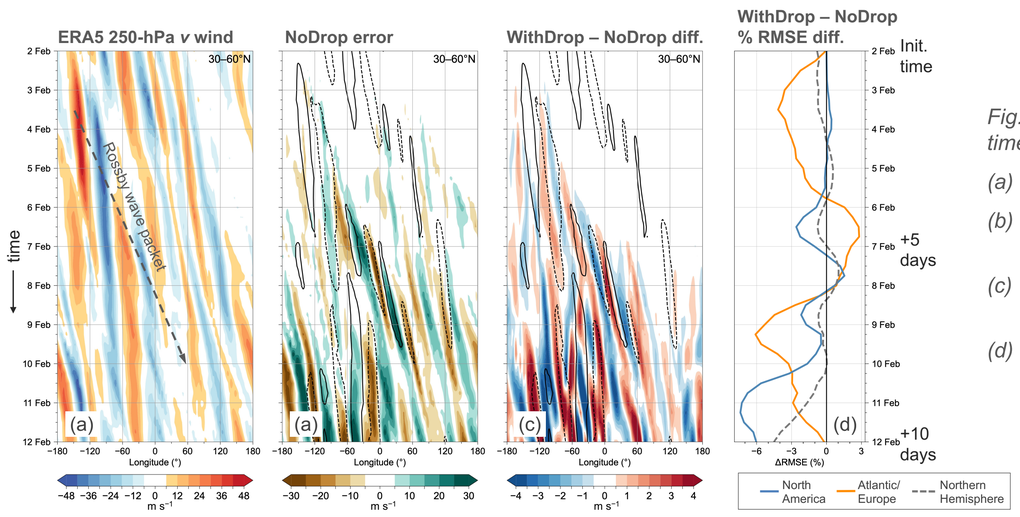

Fig. 7. 250-hPa meridional wind Hovmöller & time series plots for 30–60°N.

(a) ERA5 merid. wind

(b) NoDrop forecast errors, overlaid by NoDrop merid. wind contours (±18 m^{-1}).

(c) WithDrop – NoDrop difference, overlaid by NoDrop merid. wind contours (±18 m^{-1}).

(d) WithDrop – NoDrop % difference in the RMSE over North America (70–120°W), the Atlantic/Europe region (40°W–40°E), and the Northern Hemisphere.

AR-centered composite perspective

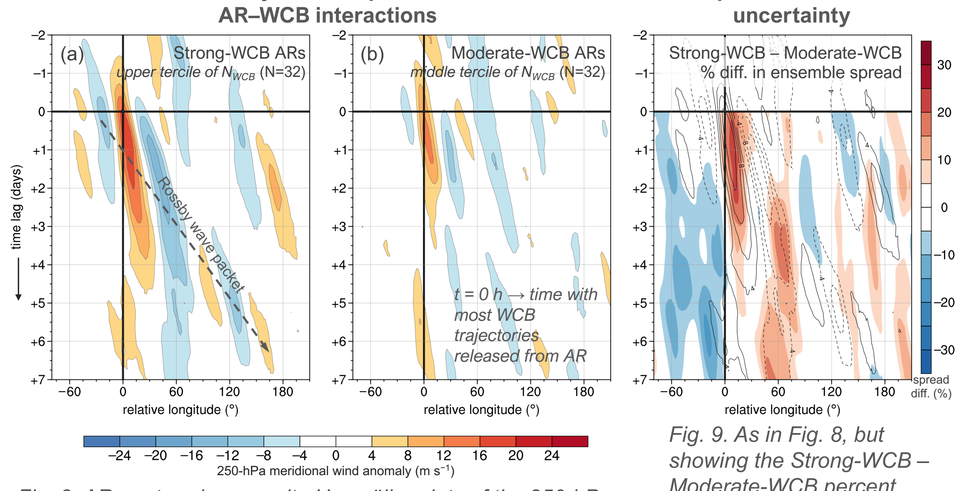

Fig. 8. AR-centered composite Hovmöller plots of the 250-hPa merid. wind anomaly (m s^{-1}, shading) averaged over 0–25° relative latitude for the (a) top tercile (Strong-WCB) and (b) middle tercile (Moderate-WCB) of ARs ranked by N_{WCB}.

Fig. 9. As in Fig. 8, but showing the Strong-WCB – Moderate-WCB percent difference in ensemble spread of 250-hPa Z from NOAA GEFS forecasts initialized at t = 0 h

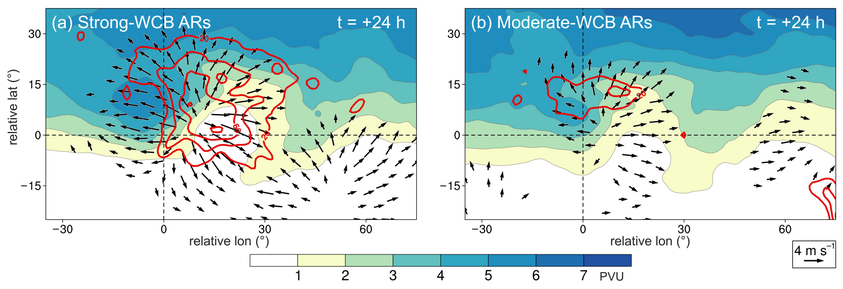

Fig. 10. AR-centered composite maps at t = + 24 h of the 250-hPa potential vorticity (PVU, shading), 250-hPa irrotational wind vectors (m s^{-1}), and AR–WCB outflow density [red contours every 20 (10^4 km^2)$^{-1}$] for (a) Strong-WCB ARs and (b) Moderate-WCB ARs.

- Strong-WCB ARs (i.e., high N_{WCB}) tend to promote the formation of coherent Rossby wave packets that propagate far downstream (Fig. 8)
- This wave response in Strong-WCB ARs arises from pronounced ridge amplification linked to WCB-related divergent outflow (Fig. 10).
- For the Strong-WCB ARs, elevated ensemble spread (from GEFS forecasts initialized at *t = 0 h* for each AR) develops and propagates downstream in conjunction with the composite wave packet (Fig. 9).